Acta Crystallographica Section D
Biological Crystallography
ISSN 0907-4449

Structure of sperm-specific protein SSP-19 from *Caenorhabditis elegans*

Norbert Schormann,[a] Jindrich Symersky[a] and Ming Luo[a,b]*

[a]Southeast Collaboratory for Structural Genomics, Center for Biophysical Sciences and Engineering, University of Alabama at Birmingham, Birmingham, Alabama, USA, and [b]Department of Microbiology, University of Alabama at Birmingham, Birmingham, Alabama, USA

Correspondence e-mail: mingluo@uab.edu

Received 4 June 2004
Accepted 20 July 2004

PDB Reference: SSP-19, 1row, r1rowsf.

Structural data are reported for SSP-19, a sperm-specific protein (SSP) family member from *Caenorhabditis elegans*. The SSP family [also known as the major sperm protein-like (MSP-like) family] contains proteins with only 107–109 amino acids, compared with 127 amino acids in the major sperm protein (MSP) family. MSP, the most abundant protein in nematode sperm, forms a dynamic actin-like cytoskeleton that provides the framework for the nematode sperm motility. *In vivo*, MSP dimers polymerize to form filaments that are constructed from two helical strands, which assemble into larger macromolecular structures. Little is known about the SSP family and a similar function is inferred from sequence and structural homology [Pfam (Protein Families Database of Alignments and HMMs) and SCOP (Structural Classification of Proteins) classification]. Despite the overall structural homology, the monomer–monomer interactions in SSP-19 are strikingly different from the interactions in the two MSP canonic domains described previously.

1. Introduction

Nematode sperm crawl like amoebae using a cytoskeleton constructed from their major sperm protein (MSP). Amoeboid locomotion is a central function of many eukaryotic cells and is usually generated by a remodeling of the actin cytoskeleton. In nematodes, however, sperm motility is produced by polymerization of MSP, a 14 kDa protein that forms filaments packing the lamellipod (Roberts & Stewart, 2000; Italiano *et al.*, 2001). Both actin and MSP use directed assembly and bundling of filaments (Buttery *et al.*, 2003). The macromolecular assembly described by Baker *et al.* (2002) takes place in a hierarchical manner. Firstly, helical subfilaments are built from MSP dimers. Secondly, two subfilaments coil around each other to form a filament. Thirdly, filaments supercoil to produce bundles. As the most abundant protein in nematode sperm, MSP accounts for about 40% of the soluble protein (Baker *et al.*, 2002). While the proteins of the MSP domain contain 127 amino acids (14 kDa), there is also a family of MSP-like proteins called sperm-specific proteins (SSP) that contain only 107–109 amino acids (11 kDa). Protein sequence information is available for seven members (SSP-9, SSP-10, SSP-11, SSP-16, SSP-19, SSP-31 and SSP-32). Little is known about this family and a similar function is suggested in SCOP (Structural Classification of Proteins) and Pfam (Protein Families Database of Alignments and HMMs) based on their structural homology with the MSP family. Crystal structures of MSP domains from *Caenorhabditis elegans* (PDB code 1grw) and *Ascaris suum* (PDB codes 1msp and 2msp) have been reported previously (Baker *et al.*, 2002; Bullock *et al.*, 1996). In addition, an NMR solution

structure of the MSP domain of *A. suum* (PDB code 3msp) is available (Haaf *et al.*, 1998). The only other structure (PDB code 1m1s) of the MSP-like domain of a member of the SSP family from *C. elegans* was recently released. Two of the structures of the MSP domain (1grw, 2msp) give a glimpse of the putative subfilament, while the other two entries (1msp, 3msp) provide a look at the conserved structure of the basic building block, the dimer. Supramolecular assemblies of the *A. suum* MSP, induced *in vitro* by ethanol were studied by electron microsopy (King *et al.*, 1994) and compared with the large filamentous superstructures observed in the sperm pseudopod (Sepsenwol *et al.*, 1989).

Here, we report the structure of another member of the SSP family and compare the observed interfaces with the previously described interactions (Bullock *et al.*, 1996; Baker *et al.*, 2002).

2. Materials and methods

2.1. Cloning, expression and purification

As a part of the structural genomics initiative on *C. elegans*, we expressed and purified an MSP-like protein, SSP-19 (AceId C55C2.2; PIR T15224). The cloning and high-throughput expression analysis of *C. elegans* open reading frames (ORFs) is described in detail elsewhere (Finley *et al.*, 2004). Briefly, *C. elegans* genes are screened using the Gateway cloning and expression system (Invitrogen) in 96-well microtiter plates. Individual genes are subcloned into the Gateway expression vector pDEST17.1, which contains a hexahistidine tag upstream of the N-terminal recombination site and a three-phase stop codon downstream of the C-terminal recombination site. This expression vector containing the *C. elegans* gene of interest (ssp-19) was transformed into *Escherichia coli* BL21(DE3) cells and protein expression was carried out for 20 h at 291 K. After thrombin cleavage of the His tag the protein still carried remaining Gateway residues at the N- and C-termini. Since the protein is small (109 residues), these extra residues (16) constitute a large percentage and have been shown to interfere with our goal of obtaining diffraction-quality crystals. To improve the quality of the crystals, the protein was subcloned using pET28b vector (Novagen) with a 20-residue N-terminal extension containing a hexahistidine tag and a thrombin-cleavage site. The target protein was fractionated by nickel-affinity chromatography and cleavage of the His tag produced the full-length domain. The protein was further purified by gel-filtration chromatography (S-75 column, Amersham Biosciences).

2.2. Crystallization and data collection

The purified protein was concentrated to 7 mg ml^{-1} (Bradford assay) in 20 m*M* HEPES buffer pH 7.5 and 0.5%(*v*/*v*) octyl β-D-glucopyranoside (Sigma). The detergent was necessary for solubilization of the protein. The protein was subjected to initial screening of crystallization conditions using two crystal screens (Hampton Research). Three conditions of the Natrix screening kit (1, 12 and 18), all of which contained varying amounts of lithium sulfate (2.0, 1.8 and 1.3 *M*, respectively) as the precipitant, produced protein crystal clusters. Crystals broken off the clusters diffracted strongly to about 1.6 Å at our X-ray home source. Indexing of the diffraction spots proved unsuccessful since the diffraction pattern resulted from multicrystalline species. After optimization of the best crystallization condition (Natrix 1), a single crystal was obtained for data collection. The crystal was grown at 295 K by hanging-drop vapor diffusion using 1 µl protein solution and 1 µl well solution (1.7 *M* lithium sulfate, 50 m*M* MES pH 5.6 and 100 m*M* $MgCl_2$). The crystal was rapidly transferred to mother liquor containing 25%(*v*/*v*) glycerol and flash-frozen in liquid nitrogen. Diffraction data were collected at 103 K on a Rigaku R-AXIS IV image-plate detector using Cu $K\alpha$ (λ = 1.5418 Å) radiation generated by a rotating-anode generator. A crystal with dimensions of 0.3 × 0.3 × 0.15 mm could be indexed in space group $P2_1$, with unit-cell parameters a = 52.35, b = 31.85, c = 55.58 Å, β = 97.67°, with rather high mosaicity (1.5°). A data set was collected to 1.8 Å resolution using an oscillation angle of 1° per frame. Data were processed

Table 1
Crystal and data-collection statistics.

Values in parentheses refer to the highest resolution shell.

Resolution range (Å)	50.00–2.20 (2.28–2.20)
Observed reflections	28027
Unique reflections	8710 (852)
Completeness (%)	92.4 (89.7)
Redundancy	3.3 (3.0)
Average $I/\sigma(I)$	35.7 (21.9)
$R_{\rm merge}$† (%)	5.3 (8.7)

† $R_{\rm merge} = \sum_j |I_j - \langle I\rangle| / \sum I_j$, where I_j is the intensity measurement for reflection j and $\langle I\rangle$ is the mean intensity for multiply recorded reflections.

Table 2
Refinement and model statistics.

Values in parentheses refer to the highest resolution shell.

Resolution range (Å)	24.79–2.20 (2.34–2.20)
Reflections used (F/σ = 0)	8637 (1217)
Completeness (%)	91.3 (84.3)
R (all reflections) (%)	21.9 (23.7)
$R_{\rm work}$†	22.4 (20.7)
$R_{\rm free}$†	28.0 (32.7)
No. protein residues	214
No. water molecules	157
Wilson B (Å^2)	30.8
Average B for all atoms (Å^2)	26.6
Average B for protein (Å^2)	25.8
Average B for water (Å^2)	34.7
R.m.s.d. bond lengths (Å)	0.007
R.m.s.d. bond angles (°)	1.30
Coordinate error (Å)	
Luzzati‡	0.26
SigmaA§	0.12
Residues in Ramachandran core region (%)	93.2

† $R_{\rm work}$, $R_{\rm free} = \sum \big||F_{\rm o}| - |F_{\rm c}|\big| / \sum |F_{\rm o}|$, where the working and free R factors are calculated using the working and free reflection sets, respectively. The free reflections (5% test set) were set aside throughout refinement. ‡ Luzzati (1952). § Read (1990).

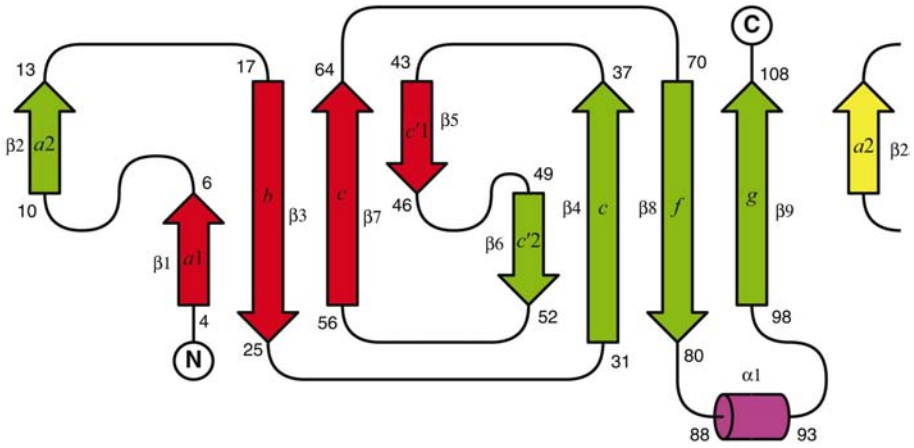

Figure 1
Topology diagram for SSP-19. N- and C-termini are shown. The secondary-structure elements are labeled and their starting and ending residue numbers are also indicated. Labeling of β-strands is performed both consecutively and using the nomenclature for the sub-class of the s-type Ig fold as described by Bullock *et al.* (1996). The two sheets are distinguished by color (sheet *A* with strands *a*1, *b*, *e* and *c*′1 in red; sheet *B* with strands *a*2, *c*′2, *c*, *f* and *g* in green). To emphasize the actual position in sheet *B*, *a*2 is repeated on the right-hand side (in yellow). The lone helix is also shown (in pink). The figure was prepared using *TOPDRAW* (Bond, 2003).

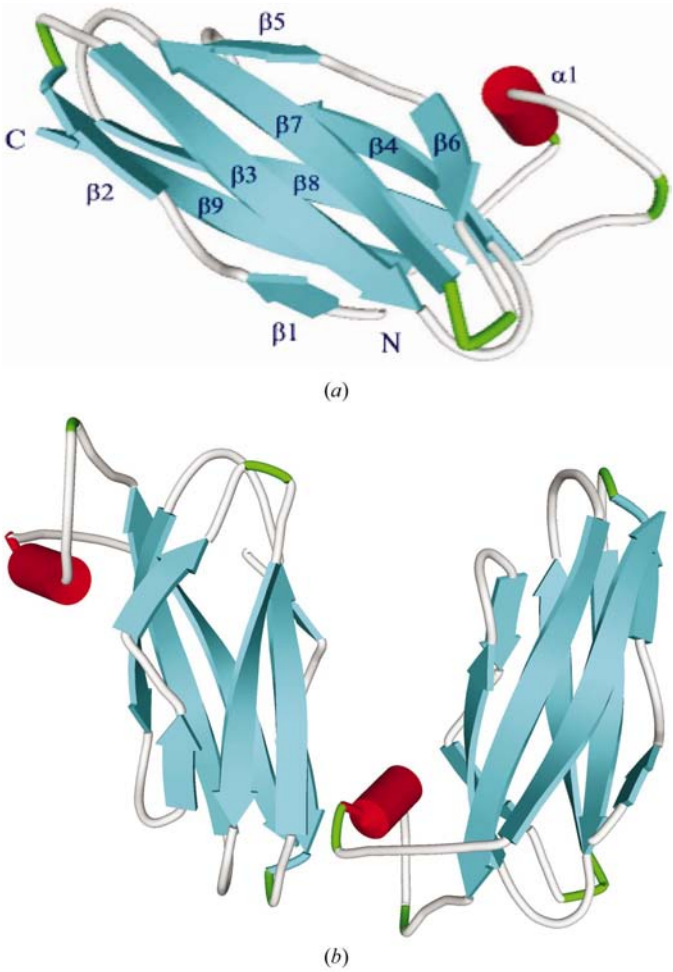

Figure 2
(*a*) Cartoon drawing of SSP-19 (chain *A*) with labels for the secondary-structure elements (consecutive labeling of the strands and the lone helix as in Fig. 1). N- and C-termini are also indicated. (*b*) Dimer interface 1 for 1row (cartoon drawing). Both figures were generated using *ViewerLite* 5.0 (Accelrys Inc.).

with *HKL*2000 (Otwinowski & Minor, 1997). Based on completeness, the data were subsequently truncated to 2.2 Å resolution (Table 1). Data quality is very good as indicated by an average $I/\sigma(I)$ of 35.7 (21.9 in the highest resolution shell) and a low $R_{\rm merge}$ (5.3% overall and 8.7% in the highest resolution shell).

2.3. Structure solution and refinement

At the time of target selection, purification and crystallization, the only available homology models (1grw and 1msp) had sequence identities of below 20%. No structure solution by molecular replacement was attempted at this time. Structure solution by molecular replacement using *MOLREP* (Vagin & Teplyakov, 1997) from the *CCP*4 suite (Collaborative Computational Project, Number 4, 1994) succeeded when PDB entry 1m1s became available. A search model of SSP-19 was created by comparative protein modelling in *MODELLER* (Sali & Blundell, 1993) using the coordinates of 1m1s, the target sequence for SSP-19 and the sequence alignment for both proteins (the r.m.s. deviation between our search model and 1m1s for 105 C^{α} atoms is 0.1 Å). A plot of the self-rotation function, the Matthews coefficient and packing considerations indicated the presence of two monomers in the asymmetric unit related by non-crystallographic twofold symmetry. A resolution cutoff of 3.5 Å was crucial for finding the right orientation of both monomers. Refinement using *CNS* v.1.1 (Brünger *et al.*, 1998) proceeded smoothly in the early stages, but in later stages parts of the model (loops and the lone α-helix) had to be rebuilt using *O* (Jones *et al.*, 1991) and *QUANTA* (Accelrys Inc.). The two chains were initially refined with non-crystallographic symmetry restraints, but were refined independently in later stages. The r.m.s. deviation between individual monomers (chains *A* and *B*) for 107 C^{α} atoms is 0.5 Å. After addition of solvent molecules, the refinement converged at an *R* factor of 22.4% ($R_{\rm free}$ of 28.0%). Refinement statistics (resolution range 24.79–2.20 Å and F/σ = 0) are shown in Table 2.

3. Results and discussion

3.1. Quality of the model

The model quality is very good as indicated by the Ramachandran plot (93% of residues in core regions) and relatively low temperature factors (average *B* factor of 26.6 $Å^2$ for all atoms). The final model consists of 107 residues each of two chains *A* and *B* related by a non-crystallographic twofold axis (a total of 214 amino-acid residues in the asymmetric unit) and 157 solvent atoms. Only the two N-terminal residues as well as the side chain of Val17 are not visible in the electron density

Table 3
Structural comparison of various MSP and MSP-like domains.

Structures were aligned using the program *TOPP* (Guoguang Lu, Karolinska Institute, Stockholm, Sweden) from the *CCP*4 suite (Collaborative Computational Project, Number 4, 1994).

	Identity (%) (No. amino acids)	Match rate (%) (No. amino acids)	R.m.s.d. (Å) (No. C^{α} atoms)
1row *versus* 1m1s	42.3 (41)	90.7 (97)	0.9 (97)
1row *versus* 1grw	19.8 (17)	80.4 (86)	1.2 (86)
1row *versus* 1msp	16.5 (15)	85.0 (91)	1.5 (91)
1grw *versus* 1msp	82.3 (102)	100 (124)	0.5 (124)

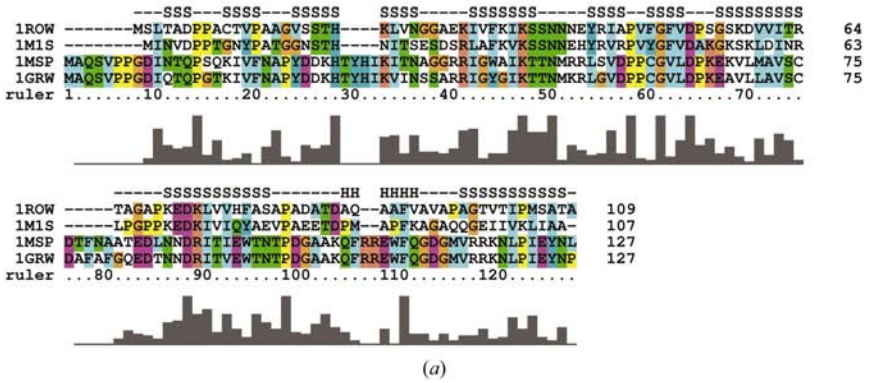

(*a*)

(*b*)

Figure 3
Sequence alignment and structural superimposition of MSP and MSP-like domains (PDB codes 1grw, 1msp, 1row and 1m1s). (*a*) Sequence comparison of MSP and MSP-like domains with overlaid secondary-structure assignment for SSP-19 (S, β-strand; H, α-helix). Color codes reflect different chemical types of amino-acid residues. The higher the bar under the alignment, the higher the conservation at the given amino-acid position. The figure was generated using *ClustalX* (Jeanmougin *et al.*, 1998). (*b*) Structural superimposition (C^{α} trace in stick representation) of MSP and MSP-like domains (see also Table 3). Color codes correspond to the different domains (1msp in red, 1grw in grey, 1m1s in yellow and 1row in cyan). The figure was generated using *ViewerLite* 5.0 (Accelrys Inc.).

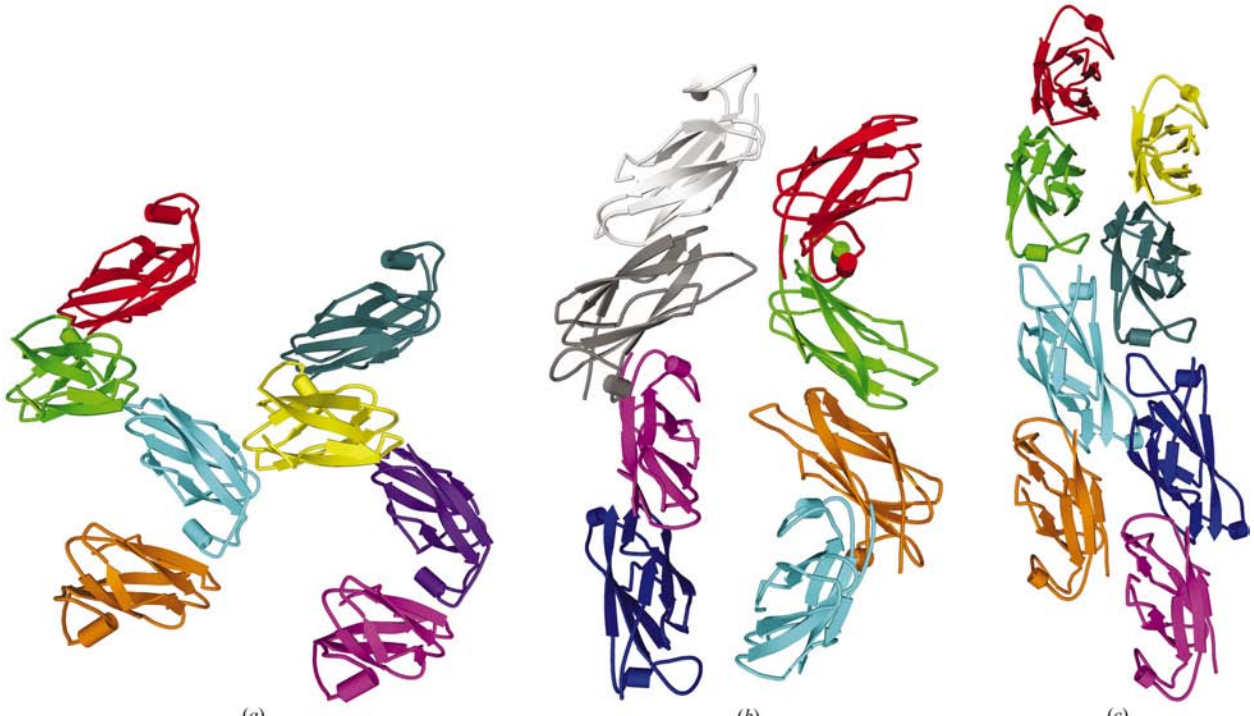

(*a*) (*b*) (*c*)

Figure 4
Interface of two adjacent helices for 1row and 1msp compared with the helical putative subfilament structure of 2msp (cartoon drawing with different chain colors). (*a*) Packing of helices for 1row. (*b*) Packing of helices for 1msp. (*c*) Putative helical subfilament structure for 2msp. The figures were generated using *ViewerLite* 5.0 (Accelrys Inc.).

for both monomers. Both *R* factors are somewhat higher than expected for 2.2 Å resolution, but this may be because of the relatively high mosaicity of the crystal. Table 2 lists the model statistics.

3.2. Overall structure

The polypeptide chain shows an immunoglobulin-like fold (Greek-key barrel) based on a seven-stranded β-sandwich. In two strands, *cis*-prolines (Pro7 and Pro47) produce distinctive kinks, resulting in nine β-strands. Fig. 1 shows the topology diagram generated by *TOPDRAW* (Bond, 2003). The nomenclature for the subclass of the s-type Ig fold as described by Bullock *et al.* (1996) is used. The nine β-strands are grouped into two sheets. The second β-strand pairs with the C-terminal β-strand and belongs to sheet *B*. Sheet *A* (antiparallel) consists of four β-strands (order: *a*1, *b*, *e*, *c*′1), sheet *B* (mixed) of five β-strands (order: *c*′2, *c*, *f*, *g*, *a*2). Fig. 2(*a*) shows a cartoon drawing for monomer *A* of 1row.

3.3. Sequence and structural comparison of all structurally characterized MSP and MSP-like domains

Sequence alignment of the two MSP-like domains with the two MSP domains shows that the MSP domains are highly homologous (83% identity), while the MSP-like domains are more variable (42% identity) and display low sequence homology (16–18% identity) to the two MSP domains (Fig. 3*a*). As expected, a structural superimposition of all four domains shows a lower r.m.s. deviation (0.9 Å for 97 C^{α} atoms) between the MSP-like domains compared with higher r.m.s. deviations between the MSP-like and MSP domains (see Table 3). Again, the MSP domains (PDB codes 1grw and 1msp) demonstrate an almost perfect structural match. Nonetheless, the core region (β-sandwich) of all MSP and MSP-like domains for which the three-dimensional models are available is structurally very well conserved (Fig. 3*b*). Differences are mainly seen in the connecting loop regions and the helical region. The additional residues of the MSP domains form extended loops and an additional helical region (Fig. 3*b*). The dimer interface and packing of the MSP-like domain of SSP-19 is unusual when compared with the related structures (1msp, 2msp) of the MSP domain (Figs. 2*b* and 4). The major interactions between monomers at the first dimer interface in the MSP domain (1msp) involve strand β2, the adjacent loop regions and the C-terminus (hydrogen bonds between Asn125 and Lys16, Asp24 and Lys32, Asn20 and Val18 of chain *A* and *B*; hydrophobic contacts between Ala21 and Pro13 of chain *A* and *B*). This interface can be seen in Fig. 4(*b*) (interactions, for instance, between the gold and green molecules). In the MSP-like domain of SSP-19 there are only a few interactions (hydrogen bond between Val93 of chain *A* and Ser18 of chain *B*; hydrophobic contacts between Ala94 of chain *A* and Val12, Pro13 and Gly17 of chain *B*). This dimer interface for SSP-19 is displayed in Figs. 2(*b*) and 4(*a*) (interactions, for instance, between the gold and cyan molecule). The second dimer interface between monomers of adjacent dimers in the MSP domain shows interactions between parts of the C-terminal helix, parts of strand β9 and the connecting loop (hydrogen bonds between Asn119, Gln110 and Asp112 of chains *A* and *C*, hydrogen bonds between Gly113 and Arg117 of chain *A* and *C*, hydrogen bond between Val115 of chain *A* and Val115 of chain *C*; hydrophobic contacts between Pro5, Met114 and Arg116 of chains *A* and *C*), while SSP-19 demonstrates only hydrophobic interactions (hydrophobic contacts between Ala15, Ala66 and Ala109 of chain *A* and Val61, Thr63 and Thr65 of chain *C*; hydrophobic contacts between Gly67, Ala68 and Pro69 of chain *A* and Gly17 and Ser18 of chain *C*). This interface can be seen in Fig. 4(*a*) (interactions, for instance, between the cyan and green molecule) and Fig. 4(*b*) (interactions, for instance, between the green and red molecule). The observed interactions result in different packing (Fig. 4). The monomer–monomer interactions in SSP-19 probably arise from crystal packing, especially since in the absence of point-group symmetry this contact would be expected to be repeated from molecule to molecule, which is not the case. Nonetheless, the superimposition of 1row with 1msp, based on sequence and structural alignment, shows that 1row cannot form the same interactions at the first dimer interface because of differences in sequence in the interacting regions. There would only be a few resulting contacts (a hydrogen bond between Thr11 of chain *A* and Thr11 of chain *B*; a hydrophobic contact between Pro7 and Ala109 of chain *A* and Pro7 and Ala109 of chain *B*). It needs to be emphasized that the protein–protein interactions in MSP domains are more extensive than in MSP-like domains. The buried solvent-accessible surface per chain is doubled (approximately 1000 $Å^2$ in 1msp compared with approximately 500 $Å^2$ in 1row). The crystal contacts in the structures that show the putative subfilaments (1grw and 2msp) occur between parallel untwisted subfilaments, while within the filaments *in vivo* and *in vitro* the interactions are between a twisted pair of subfilaments. One of these structures (2msp) contains two parallel helices of the putative subfilaments in the asymmetric unit. The structure of the basic building block, the dimer (1msp), forms parallel helices that are generated by crystallographic symmetry. The same situation occurs in our structure (1row), although the interfaces between monomers and dimers, as well as the interface between adjacent helices, are different. Two adjacent helices (chains *A*, *B*, *C*, *D* and chains *A*′, *B*′, *C*′, *D*′) in 1row interact by forming another interface through hydrogen bonds (Ala5 of chain *A* and Ala28 of chain *C*′; Thr102 of chain *A* and Gly26 of chain *C*′) and hydrophobic contacts (Pro8 of chain *A* and Glu29 of chain *C*′; Thr4 of chain *A* and Pro54 of chain *C*′; Phe78 of chain *A* and Ser55 of chain *C*′). This third interface can be seen in Fig. 4(*a*) (interactions between the cyan and yellow molecule). In 1msp, the two adjacent parallel helices (chains *A*, *B*, *C*, *D* and chains *A*′, *B*′, *C*′, *D*′) show various contacts formed between two sets of chains (hydrogen bond between Gln15 of chain *A* and Lys102 of chain *A*′; hydrogen bond between Lys102 of chain *C* and Gln15 of chain *C*′; hydrogen bonds between Gln103 of chain *A*′ and Asn85, Asp87 and Arg88 of chain *A*; hydrogen bonds between Gln103 of chain *C* and Asn85, Asp87 and Arg88 of chain *C*′; hydrogen bonds between Asn119 of chains *A* and *C*′ and Gln110 and

Asp112 of chains *C′* and *A*; hydrogen bonds between Gly113 of chains *A* and *C′* and Arg117 of chains *C′* and *A*; hydrogen bonds between Val115 of chains *A* and *C′*; hydrophobic contacts between Pro5, Met114 and Arg116 of chains *A* and *C′*). On the other hand, the interfaces between two helical subfilaments in 2msp involve numerous contacts, that are not created by the crystallographic symmetry and differ from the packing in 1msp (hydrogen bonds between Gly80 and Arg40, Gln81 and Arg40, Glu82 and Arg39; salt bridge between Asp75 and Lys102, Asp25 and Arg40; extensive hydrophobic contacts between N-terminal residues 3–5, 56–57, 78–81, 101–103 and 114–116). The packing of adjacent helices in 1row and 1msp, together with the packing of helical subfilaments in 2msp, is shown in Fig. 4.

It has to be emphasized that the other structure of an SSP family member (1m1s) shows only a monomer in the asymmetric unit and the observed packing is different from our structure. It needs to be determined whether this finding of different interactions between monomers is an exception or the rule among members of the SSP family.

4. Conclusions

Although structurally remarkably conserved compared with major sperm proteins, the two crystal structures of sperm-specific proteins show different interactions between polypeptide chains and do not conserve the dimeric assembly observed in major sperm proteins. A moderate sequence homology and a high structural homology with major sperm proteins suggest that sperm-specific proteins may have a function in filament formation. It is not clear, however, whether sperm-specific proteins can polymerize into subfilaments as described for major sperm proteins or whether they perform a different function.

The goal of this work was to provide the framework for further studies on sperm-specific proteins. The functional study of members of the SSP family is beyond the scope of this paper and our structural genomics initiative.

We thank the Structural Genomics of *C. elegans* (SGCE) group for providing the protein. The work described here was supported by NIGMS Grant IP50-M62407.

References

Baker, A. M. E., Roberts, T. M. & Stewart, M. (2002). *J. Mol. Biol.* **319**, 491–499.
Bond, C. S. (2003). *Bioinformatics*, **19**, 311–312.
Brünger, A. T., Adams, P. D., Clore, G. M., DeLano, W. L., Gros, P., Grosse-Kunstleve, R. W., Jiang, J.-S., Kuszewski, J., Nilges, M., Pannu, N. S., Read, R. J., Rice, L. M., Simonson, T. & Warren, G. L. (1998). *Acta Cryst.* D**54**, 905–921.
Bullock, T. L., Roberts, T. M. & Stewart, M. (1996). *J. Mol. Biol.* **263**, 284–296.
Buttery, S. M., Ekman, G. C., Seavy, M., Stewart, M. & Roberts, T. M. (2003). *Mol. Biol. Cell*, **14**, 5082–5088.
Collaborative Computational Project, Number 4 (1994). *Acta Cryst.* D**50**, 760–763.
Finley, J. B., Qiu, S.-H., Luan, C.-H. & Luo, M. (2004). *Protein Expr. Purif.* **34**, 49–55.
Haaf, A., LeClaire, L. III, Roberts, G., Kent, H. M., Roberts, T. M., Stewart, M. & Neuhaus, D. (1998). *J. Mol. Biol.* **284**, 1611–1624.
Italiano, J. E., Stewart, M. & Roberts, T. M. (2001). *Int. Rev. Cytol.* **202**, 1–34.
Jeanmougin, F., Thompson, J. D., Gouy, M., Higgins, D. G. & Gibson, T. J. (1998). *Trends Biochem. Sci.* **23**, 403–405.
Jones, T. A., Zou, J. Y., Cowan, S. W. & Kjeldgaard, M. (1991). *Acta Cryst.* A**47**, 110–119.
King, K. L., Stewart, M. & Roberts, T. M. (1994). *J. Cell Sci.* **107**, 2941–2949.
Luzzati, V. (1952). *Acta Cryst.* **5**, 802–810.
Otwinowski, Z. & Minor, W. (1997). *Methods Enzymol.* **276**, 307–326.
Read, R. J. (1990). *Acta Cryst.* A**46**, 900–912.
Roberts, T. M. & Stewart, M. (2000). *J. Cell Biol.* **149**, 7–12.
Sepsenwol, S., Ris, H. & Roberts, T. M. (1989). *J. Cell Biol.* **108,** 55–66.
Sali, A. & Blundell, T. L. (1993). *J. Mol. Biol.* **234**, 779–815.
Vagin, A. & Teplyakov, A. (1997). *J. Appl. Cryst.* **30**, 1022–1025.